

Observing information backflow from controllable non-Markovian multi-channels in diamond

Ya-Nan Lu,^{1,2,*} Yu-Ran Zhang,^{3,*} Gang-Qin Liu,^{1,4,†} Franco Nori,^{3,5} Heng Fan,^{1,4,6,‡} and Xin-Yu Pan^{1,4,6,§}

¹*Institute of Physics, Chinese Academy of Sciences, Beijing 100190, China*

²*School of Physical Sciences, University of Chinese Academy of Sciences, Beijing 100049, China*

³*Theoretical Quantum Physics Laboratory, RIKEN Cluster for Pioneering Research, Wako-shi, Saitama 351-0198, Japan*

⁴*Songshan Lake Materials Laboratory, Dongguan, Guangdong 523808, China*

⁵*Physics Department, University of Michigan, Ann Arbor, Michigan 48109-1040, USA*

⁶*CAS Centre of Excellence in Topological Quantum Computation, Beijing 100190, China*

Any realistic quantum system is inevitably subject to an external environment. This environment makes the open-system dynamics significant for many quantum technologies, such as entangled-state engineering^{1–3}, quantum simulation⁴, and quantum sensing⁵. The information flow of a system to its environment usually induces a Markovian process, while the backflow of information from the environment exhibits non-Markovianity⁶. The practical environment, usually consisting of a large number of degrees of freedom, is hard to control, despite some attempts on controllable transitions from Markovian to non-Markovian dynamics^{7–12}. Here, we experimentally demonstrate the engineering of multiple dissipative channels by controlling the adjacent nuclear spins of a nitrogen-vacancy centre in diamond. With a controllable non-Markovian dynamics of the open system, we observe that the quantum Fisher information flows¹³ to and from the environment using different noisy channels. Our work contributes to the developments of both noisy quantum metrology^{14–16} and quantum open systems from the viewpoints of metrologically useful entanglement.

The unavoidable interaction of a quantum open system with its environment leads to the dissipation of quantum coherence and correlations, making its dynamical behaviour a key role in many quantum technologies. According to the orientation of the information flow between the system and the environment, the time evolution of the open quantum system can be classified into either a Markovian or a non-Markovian one. A Markovian process assumes memoryless dynamics of a quantum open system, described by a dynamical semigroup with a time-independent Lindblad generator¹⁷. However, in the presence of memory effects, e.g., for a strong system-environment coupling, the Markovian approximation fails, and the non-Markovian process, deviating from a dynamical semigroup, allows for a revival of quantum features.

Owing to the memory effects and the ability of recovering quantum features, non-Markovian quantum dynamics¹⁸ opens a new perspective for applications in quantum metrology. Quantum metrology^{14,19}, an emerging quantum technology, aims to use quantum resources to yield a higher precision of statistical errors in estimating parameters compared to classical approaches. However, the useful quantum coherence and multipartite entanglement for sub-shot-noise sensitivity, quantified by the quantum Fisher information (QFI)^{20,21}, are very fragile to decoherence. Moreover, quantum metrological studies can be very different when being subject to either Markovian or non-Markovian noises¹⁵. Thus, it is important to es-

tablish an approach for characterising the non-Markovianity of the open-system dynamics by using the QFI flow between the quantum system and its environment¹³. The usual measures of non-Markovianity include: bipartite entanglement²², trace distance²³, and temporal steering²⁴. However, the metrological approach based on QFI also works on the information subflows through different dissipative channels for a class of time-local master equations¹³.

In our experiments, the open system is provided by a nitrogen-vacancy (NV) centre electron spin, its host ¹⁴N nuclear spin, and a proximal ¹³C nuclear spin in diamond (see Fig. 1a, and details of the sample are presented in Methods). The NV centre is a spin-1 system with a zero-field splitting

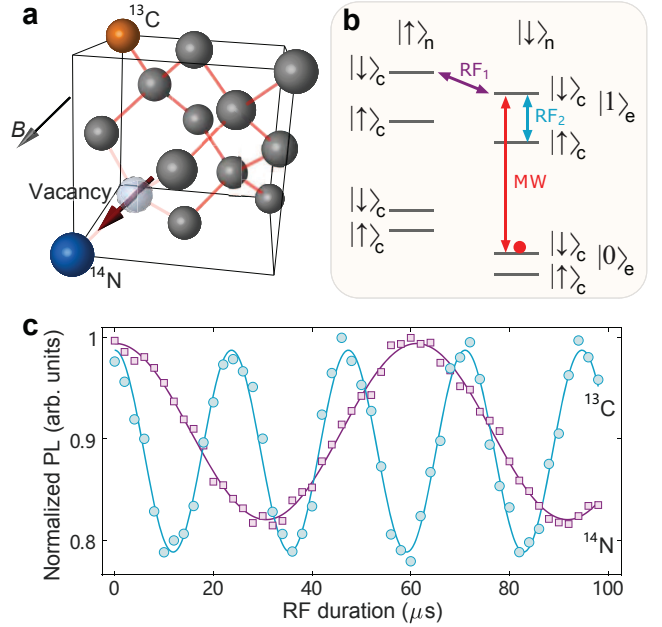


FIG. 1. Coherent manipulation of multiple spins in diamond. (a) The nitrogen-vacancy (NV) centre, its host ¹⁴N nuclear spin, and a nearby ¹³C nuclear spin form a three-qubit system. (b) Energy levels of the three-qubit system. At the excited-state level anti-crossing (ESLAC), the three spin qubits can be polarised by a short laser pulse and manipulated with resonant radio-frequency (RF) pulses (13.284 MHz for the ¹³C nuclear spin and 2.929 MHz for the host ¹⁴N nuclear spin). (c) Rabi oscillations of ¹⁴N and ¹³C nuclear spins under an external magnetic field of $B = 482$ Gauss along the quantisation axis of the NV centre (NV electron spin is at the $m_s = -1$ state).

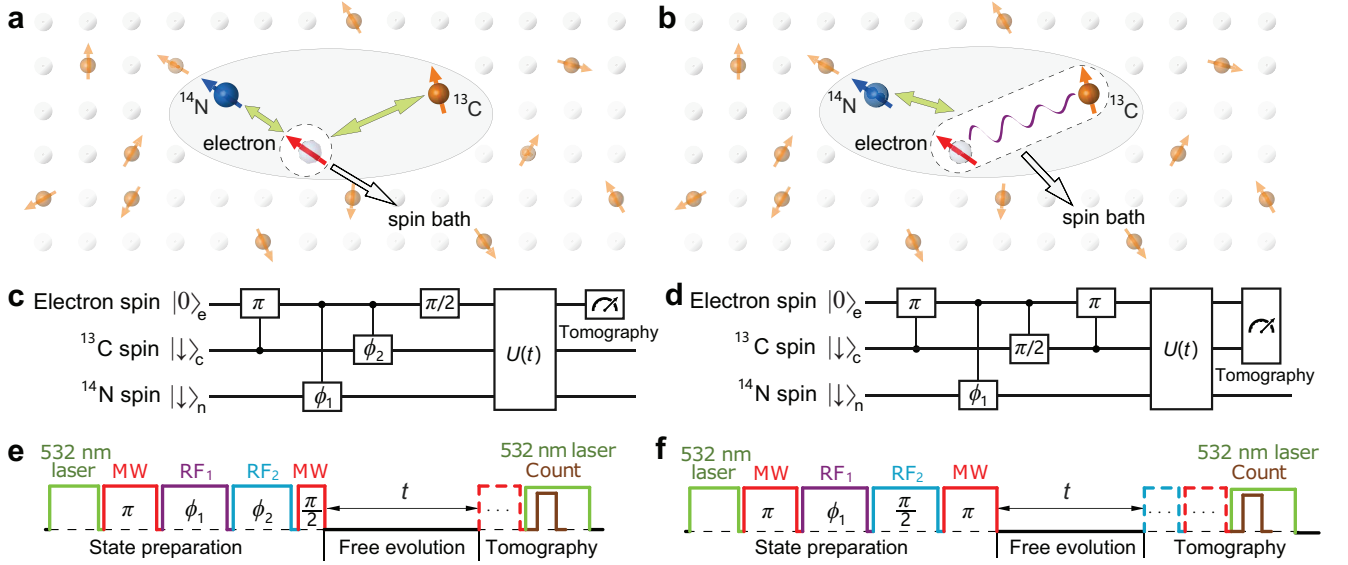


FIG. 2. **Physical coding and experimental procedures.** The NV electron spin and two strongly coupled nuclear spins play the roles of the open system and controlled dissipative channels, respectively, while the other (weakly coupled) nuclear spins form an uncontrollable dissipative channel. The quantum Fisher information (QFI) is used to characterise the quantum coherence and metrologically useful entanglement of the open system. (a) In the first experiment, the NV electron spin is the open quantum system. The quantum coherence of the system is subject to two controllable dissipative channels formed by the ^{14}N and ^{13}C nuclear spins. (b) In the second experiment, the electron spin and the ^{13}C nuclear spin form the open system, and the entanglement between the two spins is subject to a controllable dissipative channel formed by the ^{14}N nuclear spin. (c,d) Quantum circuits and (e,f) pulse sequences for the experiments. The states of the controllable channel and the open system are prepared in sequence; and state tomography of the open system, which is used to calculate the QFI and the QFI flows, is carried out after different evolution durations.

of $\Delta \simeq 2.87$ GHz between $|0\rangle_e$ and $|\pm 1\rangle_e$ of the ground spin triplet. An external magnetic field along the NV symmetry axis is applied to degenerate $|\pm 1\rangle_e$ states. Here, the first qubit is encoded on the $|0\rangle_e$ and $|-1\rangle_e$ (hereafter labelled as $|1\rangle_e$) subspace of the NV electron spin. The second and third qubits are encoded on the $|\uparrow\rangle_{n,c}$ and $|\downarrow\rangle_{n,c}$ states of the host ^{14}N nuclear spin and the nearby ^{13}C nuclear spin, respectively (see Fig. 1b for the energy levels). Applying the secular approximation and ignoring the weak nuclear-nuclear dipolar interactions, the effective interaction Hamiltonian of the three-qubit system and the spin bath can be written as²⁵ (we set $\hbar = 1$)

$$\hat{\mathcal{H}}_I = A_n^\parallel \hat{S}_e^z \hat{I}_n^z + A_c^\parallel \hat{S}_e^z \hat{I}_c^z + \hat{H}_R, \quad (1)$$

where \hat{H}_R is the interaction Hamiltonian between the electron qubit and the spin bath, $A_n^\parallel \simeq -2.16$ MHz and $A_c^\parallel \simeq 12.8$ MHz denote the hyperfine coupling strengths between the electron spin and nearby nuclear spins, respectively. Under an external magnetic field of $B_z = 482$ Gauss, the electron spin and two nuclear spins can be simultaneously polarised by a short laser pumping due to level anti-crossing in the excited state (ESLAC)²⁶. In Fig. 1c, we show Rabi oscillations of the ^{13}C and ^{14}N nuclear spins, driven by 13.284 MHz and 2.929 MHz radio-frequency (RF) pulses, respectively. We attribute the smooth and damping-free oscillations to the superb coherence of the nuclear qubits and the well-controlled driving pulses.

In our first experiment, we employ the electron qubit as a

noise sensor, whose dynamical behaviour is modulated by initialising the state of the host ^{14}N spin and the proximal ^{13}C spin (see Fig. 2a). Since the interactions between nuclear spins can be ignored in the time scale of our experiments, these two controllable nuclear spins can be regarded as the regulators of two independent dissipative channels, and other weakly coupled nuclear spins act as another uncontrollable dissipative channel (see Methods for details). The quantum circuits and pulse sequences of the first experiment are shown in Figs. 2c and 2e, respectively. By applying a 3 μs laser pulse (532 nm), these three qubits are polarised to an initial state $|\Psi_i\rangle = |0\rangle_e \otimes |\downarrow\rangle_n \otimes |\downarrow\rangle_c$. Then, by applying the MW, RF₁ and RF₂ pulses as shown in Fig. 2e, the system is prepared in $|\Psi(0)\rangle = |+\rangle_e \otimes |\psi(\phi_1)\rangle_n \otimes |\psi(\phi_2)\rangle_c$, where $|+\rangle_e \equiv (|0\rangle_e + |1\rangle_e)/\sqrt{2}$, and $|\psi(\phi)\rangle_{n,c} \equiv \cos(\frac{\phi}{2})|\uparrow\rangle_{n,c} + \sin(\frac{\phi}{2})|\downarrow\rangle_{n,c}$. The time evolution of the electron qubit can be described by the partial trace after the unitary time evolution of the total Hamiltonian $\hat{U}(t) = \exp(-i\hat{\mathcal{H}}_I t)$ as $\rho_e(t) = \text{Tr}_{\text{nrc}}[\hat{U}(t)\rho_0\hat{U}^\dagger(t)]$, where $\text{Tr}_{\text{nrc}}[\dots]$ denotes the partial trace over the host ^{14}N qubit, the 12.8 MHz ^{13}C qubit and the spin bath degrees of freedom. Given the generator $\hat{S}_e^z = \hat{\sigma}_e^z/2$, the QFI of the electron qubit can be written as

$$\mathcal{Q}(t; \phi_1, \phi_2) = r^2(t) - s_z^2(t) \simeq \mathcal{Q}_n(t; \phi_1) \mathcal{Q}_c(t; \phi_2) \mathcal{Q}_R(t), \quad (2)$$

where $r \equiv (s_x^2 + s_y^2 + s_z^2)^{1/2}$ is the length of the Bloch vector $\mathbf{r} = [s_x, s_y, s_z]$; $\mathcal{Q}_n(t) = 1 - \sin^2 \phi_1 \sin^2(A_n^\parallel t/2 + \varphi_1/2)$, $\mathcal{Q}_c(t) = 1 - \sin^2 \phi_2 \sin^2(A_c^\parallel t/2 + \varphi_2/2)$, and $\mathcal{Q}_R(t)$ are the

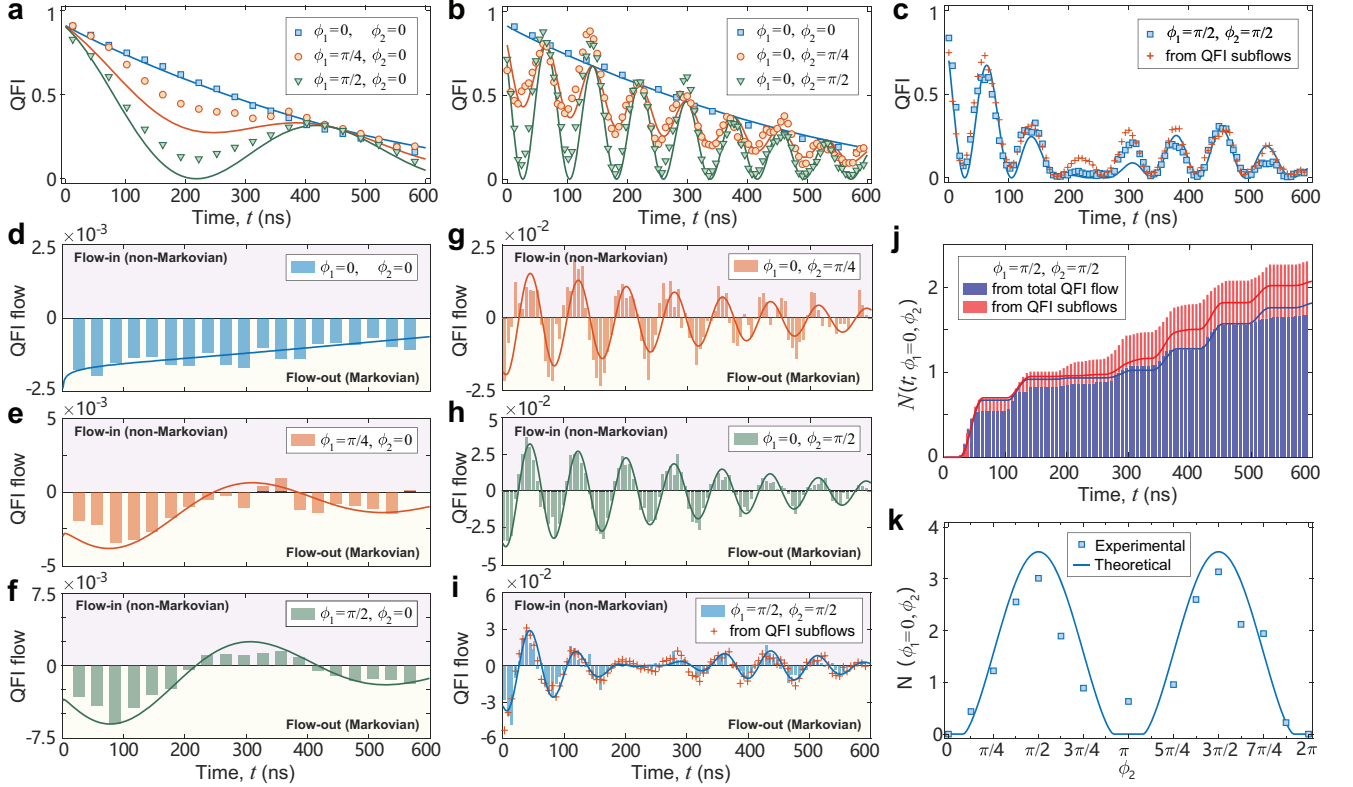


FIG. 3. **Quantum Fisher information (QFI) flows of the electron qubit in a controllable non-Markovian environment.** Time evolution of the QFI with (a) the dissipative channel of ^{14}N open ($\phi_1 = \pi/4, \pi/2$) and the one of ^{13}C closed ($\phi_2 = 0$); (b) the dissipative channel of ^{14}N closed ($\phi_1 = 0$) and the one of ^{13}C open ($\phi_2 = \pi/4, \pi/2$); (c) the dissipative channels of both nuclear spins open ($\phi_1 = \phi_2 = \pi/2$) compared with the one calculated using the results of single channels given in (a,b). QFI flows for the controllable dissipative channels with parameters: (d) $\phi_1 = \phi_2 = 0$; (e) $\phi_1 = \pi/4, \phi_2 = 0$; (f) $\phi_1 = \pi/2, \phi_2 = 0$; (g) $\phi_1 = 0, \phi_2 = \pi/4$; (h) $\phi_1 = 0, \phi_2 = \pi/2$. (i) When the dissipative channels are adjusted with parameters $\phi_1 = \phi_2 = \pi/2$, the total QFI flow is compared with the sum of subflows calculated by results in (d,f,h). (j) The measure of non-Markovianity from the total positive QFI flow in (i) compared with the measure from the QFI subflows with respect to different dissipative channels [$N(t, \frac{\pi}{2}, \frac{\pi}{2})$ in Eq. (4)], versus the evolution time. (k) The long-time non-Markovianity measure $\mathcal{N}(0, \phi_2)$ for different parameters ϕ_2 of the ^{13}C dissipative channel, when the ^{14}N channel is closed ($\phi_1 = 0$). The solid curves are for the numerical simulations using experimental parameters.

QFI of the electron qubit only subject to the ^{14}N , ^{13}C , and the spin bath dissipative channels, respectively. Details on $\mathcal{Q}_R(t)$ can be found in Methods.

The QFI flow, defined as the rate of change of the QFI, $\mathcal{I}(t) \equiv \partial_t \mathcal{Q}(t; \phi_1, \phi_2)$, can be explicitly written as a sum of QFI subflows with respect to different dissipative channels¹³

$$\mathcal{I}(t) = \mathcal{I}_n(t) + \mathcal{I}_c(t) + \mathcal{I}_R(t), \quad (3)$$

where $\mathcal{I}_i(t) \equiv \mathcal{Q}(\partial_t \ln \mathcal{Q}_i)$, with $i = n, c, R$, and each QFI subflow corresponds to not only the individual separable dissipative channel but also all channels¹³. Moreover, the inward QFI subflow ($\mathcal{I}_i > 0$), resulting from the temporary appearance of a negative decay rate²⁷ of the time-local Lindblad master equation¹⁷, is an essential feature of non-Markovian behaviours. Furthermore, we focus on the sum of time integrals of all inward QFI subflows

$$N(t, \phi_1, \phi_2) \equiv \sum_{i=n,c,R} \int_0^t \frac{|\mathcal{I}_i(\tau)| + \mathcal{I}_i(\tau)}{2} d\tau, \quad (4)$$

as a measure of non-Markovianity, and the long-time measure is defined as $\mathcal{N}(\phi_1, \phi_2) \equiv N(t \rightarrow \infty, \phi_1, \phi_2)$. Different from the time integral of the total QFI flow, the measure of non-Markovianity in Eq. (4) considers the inward subflow from each dissipative channel and can dig out the non-Markovianity even when the total QFI flow is negative.

In our experiments, the dissipative channels of the ^{14}N and ^{13}C qubits can be fully controlled by tuning the durations of the RF₁ and RF₂ pulses, i.e., to adjust ϕ_1 and ϕ_2 . When both channels are turned off, $\phi_1 = \phi_2 = 0$ (see Figs. 3a and 3b for the QFI), the dynamics of the NV electron spin is only affected by the spin bath and behaves Markovian with the QFI flowing out (see Fig. 3d). For $\phi_1 = \pi/4, \pi/2$, and $\phi_2 = 0$, the channel of the ^{14}N nuclear spin is open, and the revival of the QFI is shown in Fig. 3a, while the positive QFI flows are observed in Figs. 3e and 3f for witnessing non-Markovian dynamics. For $\phi_1 = 0$, and $\phi_2 = \pi/4, \pi/2$, the revival of the QFI and the positive QFI flows, subject to the channels of the ^{13}C nuclear spin and the spin bath, are plotted in Figs. 3b, 3g, and 3h. For fifteen experimental instances of ^{13}C qubit's

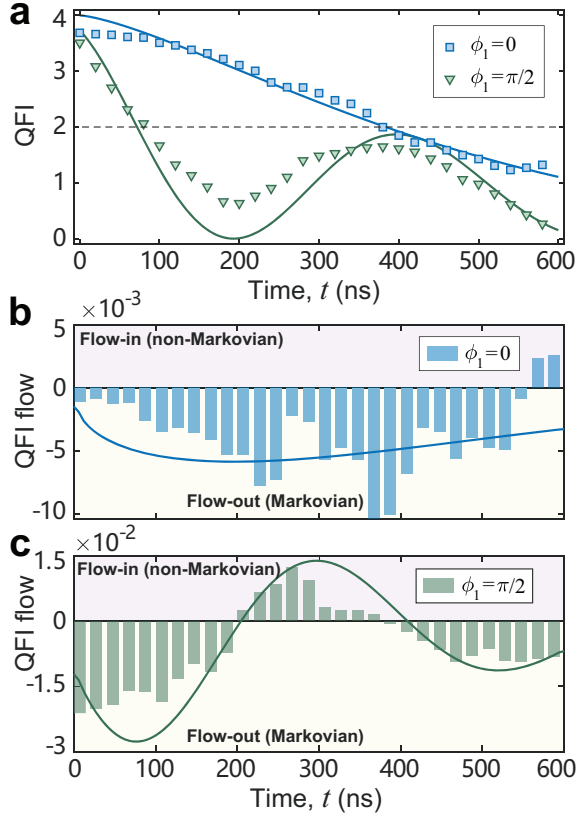


FIG. 4. **Quantum Fisher information (QFI) flows of the two-qubit maximally entangled state in a controllable non-Markovian environment.** (a) Time evolutions of the QFI of the maximally entangled state of the NV electron qubit and the 12.8 MHz ^{13}C qubit with the controllable dissipative channel of the ^{14}N qubit. QFI flows of the maximally entangled state with the controllable dissipative channel of ^{14}N (b) closed ($\phi_1 = 0$) and (c) open ($\phi_1 = \pi/2$). The solid curves are for the numerical simulations using experimental parameters.

parameter ϕ_2 , the measured $\mathcal{N}(0, \phi_2)$ is compared with the numerical simulation in Fig. 3k.

We furthermore characterise the system behaviour when both controllable dissipative channels are open. With $\phi_1 = \phi_2 = \pi/2$, the time evolution of the QFI of the electron qubit and its QFI flow, compared with the ones obtained from the sum of subflows (red cross), are shown in Figs. 3c and 3i. In Fig. 3j, the measure of non-Markovianity $\mathcal{N}(t, \frac{\pi}{2}, \frac{\pi}{2})$ from the QFI subflows, $\mathcal{I}_{n,c,R}$, with respect to different dissipative channels (red bar) is compared with the one from the total QFI flow, \mathcal{I} (blue bar). We clearly observe that the measure in terms of QFI subflows quantify more non-Markovianity than the total QFI flow, when the system is subject to multiple dissipative channels.

In the second experiment, we consider the open system, consisting of the electron qubit and the proximal ^{13}C qubit, which is subject to the controllable noisy channel of the host ^{14}N qubit and the dissipative channel of the spin bath (see Fig. 2b). Figures 2d and 2f show the quantum circuit and pulse sequences of the second experiment. Starting with the

state $|\Psi_i\rangle = |0\rangle_e \otimes |\downarrow\rangle_n \otimes |\downarrow\rangle_c$, the system is prepared in $|\Psi'(0)\rangle = (|0\rangle_e \otimes |\downarrow\rangle_c + |1\rangle_e \otimes |\uparrow\rangle_c) \otimes |\psi(\phi_1)\rangle_n$, with the pulse sequences shown in Figs. 2d and 2f. The electron qubit and ^{13}C nuclear qubit are maximally entangled at this stage. Similarly, assuming $\rho'_0 = |\Psi'(0)\rangle\langle\Psi'(0)| \otimes \rho_R$, the time evolution of the electron qubit and the ^{13}C qubit is described as $\rho'_{ec}(t) = \text{Tr}_{nR}[\hat{U}(t)\rho'_0\hat{U}^\dagger(t)]$, where $\text{Tr}_{nR}[\dots]$ denotes the partial trace over the ^{14}N spin and the spin bath degrees of freedom. If the QFI of a two-qubit state, with $(\hat{S}_e^z + \hat{S}_c^z)$ being the generator, is larger than 2, i.e., $\mathcal{Q}'(t; \phi_1) > 2$, it characterises the useful entanglement for quantum-enhanced parameter estimation¹⁴.

The time evolution of the QFI of the maximally entangled state is shown in Fig. 4a, when the controllable ^{14}N channel is either closed ($\phi_1 = 0$) or open ($\phi_1 = \pi/2$). At time $t = 0$ with $\phi_1 = 0$, we obtain the maximum QFI, $\mathcal{Q}'(0; 0) = 3.687$, which is useful for sub-shot-noise-limit metrology^{14,28}. With the dissipative channel of ^{14}N closed ($\phi_1 = 0$), the QFI flow remains negative, except for few time intervals due to the quantum fluctuations (see Fig. 4b). In Fig. 4c, the positive QFI flow of the maximally entangled state, with $\phi_1 = \pi/2$, clearly signals the non-Markovian dynamics of the two-qubit open system. Moreover, the metrologically useful entanglement [$\mathcal{Q}'(t; \phi_1) > 2$] survives for a period of time ($\lesssim 380$ ns) with respect to the Markovian noise of the spin bath. However, it decays faster under the impact of non-Markovian noise by setting $\phi_1 = \pi/2$.

Our experiments clearly demonstrate the engineering of the non-Markovian dynamics of open systems by manipulating the electron spin, the host ^{14}N , and the neighbouring ^{13}C nuclear spins of the NV centre in diamond at room temperature. First, the electron qubit, as an open system, is subject to two controllable dissipative channels of nearby nuclear qubits, of which the QFI flow characterises the non-Markovianity and can be decomposed into subflows from individual channels. Second, when the open system, consisting of the electron qubit and the ^{13}C qubit, is prepared in the maximally entangled state, the controllable non-Markovian behaviour of the decoherence dynamics of the entanglement witnessed by the QFI flow is reported. By using the QFI as a witness for quantum coherence and metrologically useful entanglement, our work will contribute to the developments of both noisy quantum metrology and the non-Markovian dynamics of quantum open systems in solids²⁸.

Acknowledgements We would like to acknowledge Zi-Yong Ge and Qing Ai for helpful discussions, and Da Wei Lu for the codes of maximum likelihood estimation. This work was supported by the National Key Research and Development Program of China (Grant Nos. 2019YFA0308100, 2016YFA0302104, 2016YFA0300600), Strategic Priority Research Program of Chinese Academy of Sciences (Grant No. XDB28000000), and NSFC (Grant Nos. 11974020, 11934018, 11574386). Y.R.Z. was supported by the China Postdoctoral Science Foundation (Grant No. 2018M640055) and the JSPS Postdoctoral Fellowship (Grant No. P19326). F.N. was supported in part by: the AFOSR (Grant No. FA9550-14-1-0040), the ARO (Grant No. W911NF-18-

1-0358), the JST Q-LEAP program, the JST CREST (Grant No. JPMJCR1676), the JSPS-RFBR (Grant No. 17-52-50023), the JSPS-FWO (Grant No. VS.059.18N), the RIKEN-AIST Challenge Research Fund, FQXi, and the NTT PHI Lab.

Author Contributions G.Q.L., X.Y.P., and H.F. supervised the project. Y.R.Z. and G.Q.L. conceived the idea. Y.R.Z., Y.N.L., and G.Q.L. designed the experimental schemes. Y.N.L. carried out the experimental measurements. Y.R.Z., Y.N.L., and G.Q.L. analysed the data. Y.R.Z. and Y.N.L. performed the numerical simulations. Y.R.Z., Y.N.L., G.Q.L., and F.N. wrote the manuscript. All authors commented on the manuscript.

Competing Interests The authors declare no competing interests.

METHODS

QFI flow and non-Markovianity. Consider a mixed state $\rho = \sum_j \lambda_j |j\rangle\langle j|$, with $\langle i|j\rangle = \delta_{ij}$ and a generator \hat{O} , the QFI of a state $\rho(\theta) = \exp(-i\theta\hat{O})\rho\exp(-i\theta\hat{O})$ with respect to a parameter θ can be written as²⁰

$$\mathcal{Q} = 2 \sum_{\lambda_i + \lambda_j \neq 0} \frac{(\lambda_i - \lambda_j)^2}{\lambda_i + \lambda_j} |\langle i|\hat{O}|j\rangle|^2.$$

For a single qubit, any state can be expressed as

$$\rho = \mathbb{I}/2 + \sum_{\alpha=x,y,z} s_\alpha \hat{\sigma}_\alpha/2,$$

with $\mathbf{r} = [s_x, s_y, s_z]$ being the Bloch vector and $r \equiv (s_x^2 + s_y^2 + s_z^2)^{1/2}$ being the Bloch length. The QFI with respect to the generator $\hat{O} = \hat{\sigma}_z/2$ can be calculated as $\mathcal{Q} = r^2 - s_z^2$. For a qubit state with $\mathbf{s} = [1, 0, 0]$, its QFI can be calculated to be 1. The QFI plays a central role in quantum metrology and multipartite entanglement witness²⁹⁻³¹, which is also sufficient for measuring non-Markovianity¹³.

We then consider a quantum process, described by a time-local master equation^{17,27}

$$\frac{\partial \rho}{\partial t} = -i[\hat{H}, \rho] + \sum_j \gamma_j \left(\hat{A}_j \rho \hat{A}_j^\dagger - \{\hat{A}_j^\dagger \hat{A}_j, \rho\}/2 \right),$$

where \hat{H} is the Hamiltonian for the open system without coupling to the bath, $\gamma_j(t)$ is the time-dependent decay rate, and $\hat{A}_j(t)$ is the time-dependent Lindblad operator. The QFI flow of the quantum open system can be divided into different subchannels as¹³ $\mathcal{I} \equiv \partial \mathcal{Q}/\partial t = \sum_j \mathcal{I}_j$, with $\mathcal{I}_j = \gamma_j(t) \mathcal{J}_j$, and $\mathcal{J}_j \leq 0$. Therefore, the existence of any positive QFI subflow characterises a quantum non-Markovian process based on the completely positive divisibility¹⁷.

Measure of non-Markovianity via QFI subflows. From Eq. (4), the non-Markovianity can be witnessed by the sum of time integrals of all inward QFI subflows. When $\phi_1 =$

$\phi_2 = \pi/2$, QFI subflows $\mathcal{I}_n(t)$, $\mathcal{I}_c(t)$ and $\mathcal{I}_R(t)$ can be calculated from QFI with different parameters: $\mathcal{Q}_R \equiv \mathcal{Q}(t, 0, 0)$, $\mathcal{Q}_{nR} \equiv \mathcal{Q}(t, 0, \pi/2)$, and $\mathcal{Q}_{cR} \equiv \mathcal{Q}(t, 0, \pi/2)$, which can be expressed, with $\dot{\mathcal{Q}} \equiv \partial \mathcal{Q}/\partial t$, as

$$\begin{aligned} \mathcal{I}_n &= (\dot{\mathcal{Q}}_{nR} - \mathcal{Q}_{nR} \dot{\mathcal{Q}}_R / \mathcal{Q}_R) \mathcal{Q}_{cR} / \mathcal{Q}_R, \\ \mathcal{I}_c &= (\dot{\mathcal{Q}}_{cR} - \mathcal{Q}_{cR} \dot{\mathcal{Q}}_R / \mathcal{Q}_R) \mathcal{Q}_{nR} / \mathcal{Q}_R, \\ \mathcal{I}_R &= \mathcal{Q}_{cR} \mathcal{Q}_{nR} \dot{\mathcal{Q}}_R / \mathcal{Q}_R^2. \end{aligned}$$

Setup and sample. Our experiments are performed under ambient conditions on a high-purity bulk diamond (Element Six, with N concentration < 5 p.p.b., and natural abundance of ^{13}C isotopes). The NV centre is located $10 \mu\text{m}$ below the diamond surface. To enhance the photon collection efficiency of the NV centre, solid immersion lenses (SILs) are etched on the diamond surface³². The photon detection rate is 450 kcps, when the laser (532 nm) excitation power is $240 \mu\text{W}$.

We use the ODMR to detect nuclear spins, which are strongly coupled to the NV electron spin. From the continuous-wave ODMR spectrum under a small magnetic field $B \simeq 40$ Gauss (see Extended Data Figs. 1a and 1b), the host ^{14}N nuclear spin and the nearby ^{13}C nuclear spin with 12.8 MHz coupling strength are identified³³. To identify the nuclear spin with a weaker coupling strength, the external magnetic field is tuned to 482 Gauss (along the quantisation axis of the NV centre), and both the host ^{14}N and the 12.8 MHz ^{13}C nuclear spins can be polarised by a short laser pulse. We then measure the pulsed-ODMR spectra of the NV centre (see Extended Data Fig. 1c). By reducing the MW power, two other ^{13}C nuclear spins are resolved (see Extended Data Fig. 1d). The hyperfine splittings caused by these two ^{13}C nuclear spins are 0.9 MHz and 0.4 MHz, respectively. These two nuclear spins are partially polarised by the laser pumping (see Extended Data Fig. 1d), which is consistent with the literature results³⁴. In our experiments, the 12.8 MHz ^{13}C nuclear spin and the ^{14}N nuclear spin are taken as fully controllable decoherence channels, while the other nearby weakly-coupled ^{13}C nuclear spins behave as uncontrollable decoherence channels.

Coherent manipulation of the NV centre. The electron spin and nuclear spins are manipulated by the resonant MW and RF pulses. Extended Data Fig. 1e shows a typical Rabi oscillation signal of the NV electron spin, with Rabi frequency 23.8 MHz. Extended Data Fig. 1f shows the Ramsey oscillation from a deliberate MW detuning (2 MHz) and the beating between different transitions, according to the state of the 0.4 MHz ^{13}C nuclear spin. By fitting the Ramsey signal, we obtain the coherence time of this NV centre as $T_2^* \approx 2.9 \mu\text{s}$.

State tomography. The sequence to realise the single-qubit state tomography can be divided into three parts: (i) Directly collect fluorescence photon counts L_z ; (ii) prepare the state, apply a $\pi/2$ MW pulse along the x -axis, and then collect the fluorescence photon counts L_y ; (iii) prepare the state, apply a $\pi/2$ MW pulse along the y -axis, and then collect the fluorescence photon counts L_x . In addition, we collect the fluores-

cence photon counts L_0 in the bright state ($m_s = 0$), and L_1 in the dark state ($m_s = -1$), as references to normalise the fluorescence signal. With the signals on different bases, we can reconstruct the state by calculating the Bloch vector $\mathbf{r} = [s_x, s_y, s_z]$ with

$$s_x = -(2L_x - L_0 - L_1)/(L_0 - L_1), \quad (5)$$

$$s_y = (2L_y - L_0 - L_1)/(L_0 - L_1), \quad (6)$$

$$s_z = (2L_z - L_0 - L_1)/(L_0 - L_1). \quad (7)$$

The two-qubit state tomography technique is based on the single-qubit state tomography method. The key point is to apply one or two additional transfer pulses (RF/MW pulses, see concrete sequences in Ref.³⁵) to divide the full 4×4 density matrix of two qubits into several 2×2 reduced density matrices. Then, we can in turn obtain the real and imaginary parts of each element of the density matrix by implementing the single-qubit state tomography in each working transition (see Refs.^{35,36}).

QFI envelope induced by the spin bath. To quantitatively describe the influence of the spin bath on the dynamics of the quantum open system, we measure the long-term QFI of the NV electron spin, when all the controllable channels (12.8 MHz ^{13}C and 2.16 MHz ^{14}N) are turned off after polarising by a short laser (see Extended Data Fig. 2b). In Extended Data Figs. 2a and 2b, we find that the coherence and QFI decay non-monotonously, with a 0.4 MHz oscillation. We attribute this oscillation to the effects of the partially polarised

^{13}C nuclear spin, of which the hyperfine coupling strength is 0.4 MHz, and the quantisation axis is not the same as the NV electron spin's³⁴. Therefore, we can only regard the 0.4 MHz ^{13}C nuclear spin as an uncontrollable quantum channel and fit the experimental results using the formula

$$Q_R(t) = \exp[-(t/T_2^*)^\alpha][1 - \sin^2 \phi_0 \sin^2(A_{c0}^\parallel t/2 + \varphi_0/2)],$$

with $\alpha = 0.89$, $T_2^* \simeq 1026$ ns, $\phi_0 = 0.37\pi$, $A_{c0}^\parallel = 0.4$ MHz, and $\varphi_0 = 0.21\pi$. However, within the time scale of our experiments (0–600 ns), the dissipative channel of the 0.4 MHz ^{13}C nuclear spin behaves Markovian, which can be included in the Markovian channel of the spin bath (see Extended Data Fig. 2b).

Data processing. The measurements in our experiments are repeated at least 4×10^5 times to obtain a good signal-to-noise ratio. In the first experiment, each data point of the QFI is calculated from the measured photon counts (L_x , L_y , L_z , L_0 , and L_1) using Eqs. (5–7). After calculating the QFI, we smooth the data by averaging 5 data points around each specific point (the adjacent average smoothing method) to calculate the QFI flow. In the second experiment, each data point of the QFI is obtained from the full 4×4 density matrix of two qubits. The final density matrix is extracted from the measured photon counts, according to the two-qubit state tomography technique, and optimised by a maximum likelihood estimation (MLE) to reduce measurement errors.

* These authors contributed equally to this work.

† gqliu@iphy.ac.cn

‡ hfan@iphy.ac.cn

§ xypan@aphy.iphy.ac.cn

¹ C. E. Bradley, J. Randall, M. H. Abobeih, R. C. Berrevoets, M. J. Degen, M. A. Bakker, M. Markham, D. J. Twitchen, and T. H. Taminiau, “A ten-qubit solid-state spin register with quantum memory up to one minute,” *Phys. Rev. X* **9**, 031045 (2019).

² A. Omran, H. Levine, A. Keesling, G. Semeghini, T. T. Wang, S. Ebadi, H. Bernien, A. S. Zibrov, H. Pichler, S. Choi, J. Cui, M. Rossignolo, P. Rembold, S. Montangero, T. Calarco, M. Endres, M. Greiner, V. Vuletić, and M. D. Lukin, “Generation and manipulation of Schrödinger cat states in Rydberg atom arrays,” *Science* **365**, 570 (2019).

³ C. Song, K. Xu, H. Li, Y.-R. Zhang, X. Zhang, W. Liu, Q. Guo, Z. Wang, W. Ren, J. Hao, H. Feng, H. Fan, D. Zheng, D.-W. Wang, H. Wang, and S.-Y. Zhu, “Generation of multi-component atomic Schrödinger cat states of up to 20 qubits,” *Science* **365**, 574 (2019).

⁴ I. M. Georgescu, S. Ashhab, and F. Nori, “Quantum simulation,” *Rev. Mod. Phys.* **86**, 153–185 (2014).

⁵ C. L. Degen, F. Reinhard, and P. Cappellaro, “Quantum sensing,” *Rev. Mod. Phys.* **89**, 035002 (2017).

⁶ H.-P. Breuer and F. Petruccione, *The theory of open quantum systems* (Oxford University Press, 2007).

⁷ C. J. Myatt, B. E. King, Q. A. Turchette, C. A. Sackett, D. Kielpinski, W. M. Itano, C. Monroe, and D. J. Wineland, “Decoherence

of quantum superpositions through coupling to engineered reservoirs,” *Nature* **403**, 269–273 (2000).

⁸ B.-H. Liu, L. Li, Y.-F. Huang, C.-F. Li, G.-C. Guo, E.-M. Laine, H.-P. Breuer, and J. Piilo, “Experimental control of the transition from Markovian to non-Markovian dynamics of open quantum systems,” *Nat. Phys.* **7**, 931 (2011).

⁹ M. Gessner, M. Ramm, T. Pruttivarasin, A. Buchleitner, H.-P. Breuer, and H. Häffner, “Local detection of quantum correlations with a single trapped ion,” *Nat. Phys.* **10**, 105 (2013).

¹⁰ J. F. Haase, P. J. Vetter, T. Unden, A. Smirne, J. Rosskopf, B. Naydenov, A. Stacey, F. Jelezko, M. B. Plenio, and S. F. Huelga, “Controllable non-Markovianity for a spin qubit in diamond,” *Phys. Rev. Lett.* **121**, 060401 (2018).

¹¹ G. Andersson, B. Suri, L. Guo, T. Aref, and P. Delsing, “Non-exponential decay of a giant artificial atom,” *Nat. Phys.* **15**, 1123–1127 (2019).

¹² K.-D. Wu, Z. Hou, G.-Y. Xiang, C.-F. Li, G.-C. Guo, D. Dong, and F. Nori, “Detecting non-Markovianity via quantified coherence: Theory and experiments,” *arXiv:1903.03359* (2019).

¹³ X. M. Lu, X. G. Wang, and C. P. Sun, “Quantum Fisher information flow and non-Markovian processes of open systems,” *Phys. Rev. A* **82**, 042103 (2010).

¹⁴ V. Giovannetti, S. Lloyd, and L. Maccone, “Advances in quantum metrology,” *Nat. Photon.* **5**, 222–229 (2011).

¹⁵ A. W. Chin, S. F. Huelga, and M. B. Plenio, “Quantum metrology in non-Markovian environments,” *Phys. Rev. Lett.* **109**, 233601 (2012).

- ¹⁶ Z.-P. Liu, J. Zhang, Ş. K. Özdemir, B. Peng, H. Jing, X.-Y. Lü, C.-W. Li, L. Yang, F. Nori, and Y.-X. Liu, “Metrology with \mathcal{PT} -symmetric cavities: Enhanced sensitivity near the \mathcal{PT} -phase transition,” *Phys. Rev. Lett.* **117**, 110802 (2016).
- ¹⁷ H.-P. Breuer, E.-M. Laine, J. Piilo, and B. Vacchini, “Colloquium: Non-Markovian dynamics in open quantum systems,” *Rev. Mod. Phys.* **88**, 021002 (2016).
- ¹⁸ W.-M. Zhang, P.-Y. Lo, H.-N. Xiong, M. W.-Y. Tu, and F. Nori, “General non-Markovian dynamics of open quantum systems,” *Phys. Rev. Lett.* **109**, 170402 (2012).
- ¹⁹ L. Pezzè, A. Smerzi, M. K. Oberthaler, R. Schmied, and P. Treutlein, “Quantum metrology with nonclassical states of atomic ensembles,” *Rev. Mod. Phys.* **90**, 035005 (2018).
- ²⁰ S. L. Braunstein and C. M. Caves, “Statistical distance and the geometry of quantum states,” *Phys. Rev. Lett.* **72**, 3439–3443 (1994).
- ²¹ J. Ma, X. G. Wang, C. P. Sun, and F. Nori, “Quantum spin squeezing,” *Phys. Rep.* **509**, 89–165 (2011).
- ²² Á. Rivas, S. F. Huelga, and M. B. Plenio, “Entanglement and non-Markovianity of quantum evolutions,” *Phys. Rev. Lett.* **105**, 050403 (2010).
- ²³ H.-P. Breuer, E.-M. Laine, and J. Piilo, “Measure for the degree of non-Markovian behavior of quantum processes in open systems,” *Phys. Rev. Lett.* **103**, 210401 (2009).
- ²⁴ S.-L. Chen, N. Lambert, C.-M. Li, A. Miranowicz, Y.-N. Chen, and F. Nori, “Quantifying non-Markovianity with temporal steering,” *Phys. Rev. Lett.* **116**, 020503 (2016).
- ²⁵ M. W. Doherty, N. B. Manson, P. Delaney, F. Jelezko, J. Wrachtrup, and L. C. L. Hollenberg, “The nitrogen-vacancy colour centre in diamond,” *Phys. Rep.* **528**, 1–45 (2013).
- ²⁶ V. Jacques, P. Neumann, J. Beck, M. Markham, D. Twitchen, J. Meijer, F. Kaiser, G. Balasubramanian, F. Jelezko, and J. Wrachtrup, “Dynamic polarization of single nuclear spins by optical pumping of nitrogen-vacancy color centers in diamond at room temperature,” *Phys. Rev. Lett.* **102**, 057403 (2009).
- ²⁷ Á. Rivas, S. F. Huelga, and M. B. Plenio, “Quantum non-Markovianity: Characterization, quantification and detection,” *Rep. Prog. Phys.* **77**, 094001 (2014).
- ²⁸ G.-Q. Liu, Y.-R. Zhang, Y.-C. Chang, J.-D. Yue, H. Fan, and X.-Y. Pan, “Demonstration of entanglement-enhanced phase estimation in solid,” *Nat. Commun.* **6**, 6726 (2015).
- ²⁹ G. Tóth, “Multipartite entanglement and high-precision metrology,” *Phys. Rev. A* **85**, 022322 (2012).
- ³⁰ L. Pezzè and A. Smerzi, “Entanglement, nonlinear dynamics, and the Heisenberg limit,” *Phys. Rev. Lett.* **102**, 100401 (2009).
- ³¹ Y.-R. Zhang, Y. Zeng, H. Fan, J. Q. You, and F. Nori, “Characterization of topological states via dual multipartite entanglement,” *Phys. Rev. Lett.* **120**, 250501 (2018).
- ³² L. Marseglia, J. P. Hadden, A. C. Stanley-Clarke, J. P. Harrison, B. Patton, Y.-L. D. Ho, B. Naydenov, F. Jelezko, J. Meijer, P. R. Dolan, J. M. Smith, J. G. Rarity, and J. L. O’Brien, “Nanofabricated solid immersion lenses registered to single emitters in diamond,” *Appl. Phys. Lett.* **98**, 133107 (2011).
- ³³ B. Smeltzer, L. Childress, and A. Gali, “ ^{13}C hyperfine interactions in the nitrogen-vacancy centre in diamond,” *New J. Phys.* **13**, 025021 (2011).
- ³⁴ A. Dréau, J.-R. Maze, M. Lesik, J.-F. Roch, and V. Jacques, “High-resolution spectroscopy of single NV defects coupled with nearby ^{13}C nuclear spins in diamond,” *Phys. Rev. B* **85**, 134107 (2012).
- ³⁵ G.-Q. Liu, H. C. Po, J.-F. Du, R.-B. Liu, and X.-Y. Pan, “Noise-resilient quantum evolution steered by dynamical decoupling,” *Nat. Commun.* **4**, 2254 (2013).
- ³⁶ T. van der Sar, Z. H. Wang, M. S. Blok, H. Bernien, T. H. Taminiau, D. M. Toyli, D. A. Lidar, D. D. Awschalom, R. Hanson, and V. V. Dobrovitski, “Decoherence-protected quantum gates for a hybrid solid-state spin register,” *Nature* **484**, 82–86 (2012).

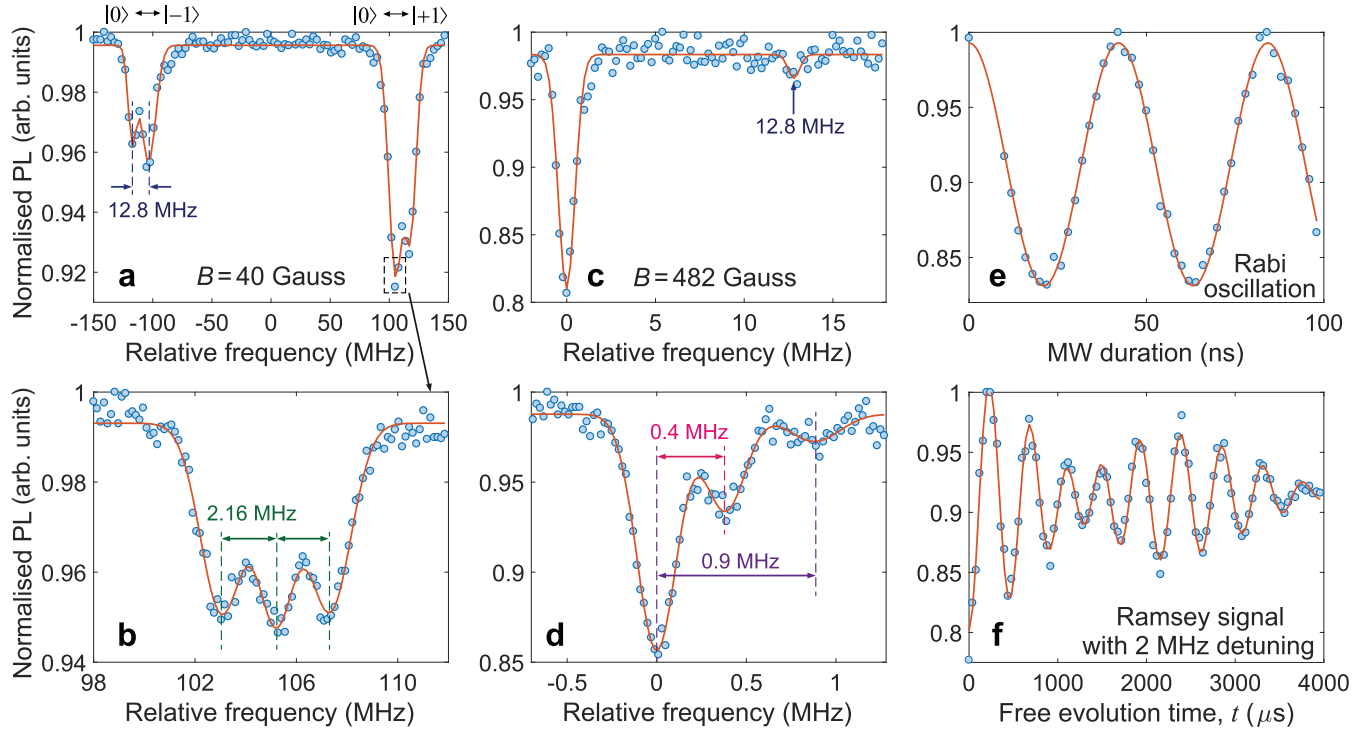


FIG. Extended Data 1. **Characterisation of the multi-qubit system.** (a,b) Continuous-wave ODMR spectra under a small magnetic field with $B = 40$ Gauss (frequency is relative to 2,870 MHz). The 2.16 MHz and 12.8 MHz splittings are induced by the ^{14}N nuclear spin and the nearby ^{13}C nuclear spin, respectively. (c,d) Pulsed-ODMR spectra under a magnetic field with $B = 482$ Gauss (frequency is relative to 1,518 MHz). Both the host ^{14}N nuclear spin and the 12.8 MHz ^{13}C nuclear spin are polarised due to ESLAC, and two other nuclear spins (0.9 MHz and 0.4 MHz) can be resolved. (e) The Rabi oscillation and (f) Free induction decay of the NV electron spin (with 2 MHz detuning). The coherence time of the NV electron spin is $T_2^* \simeq 2.9 \mu\text{s}$.

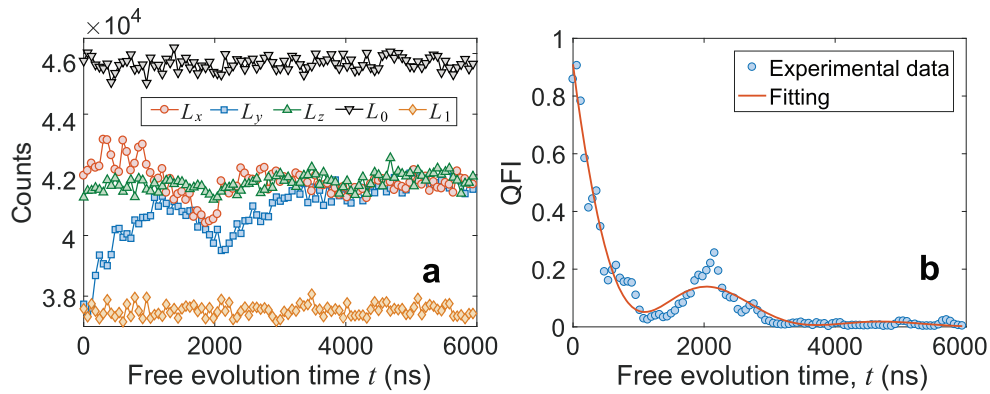


FIG. Extended Data 2. **Long-time QFI of the electron spin coupled to the uncontrolled spin bath.** (a) Measured fluorescence photon counts as functions of the free evolution time. (b) QFI of the electron qubit as a function of the evolution time, where the oscillation is induced by the nearby partially polarised 0.4 MHz ^{13}C nuclear spin.